Photochemistry and Photobiology, 2015, 91: 1348–1355

Amino Acid–Porphyrin Conjugates: Synthesis and Study of their Photophysical and Metal Ion Recognition Properties

Albish K. Paul[1], Suneesh C. Karunakaran[1], Joshy Joseph*[1,2] and Danaboyina Ramaiah*[1,3]

[1]Photosciences and Photonics Section, Chemical Sciences and Technology Division, CSIR-National Institute for Interdisciplinary Science and Technology, Thiruvananthapuram, Kerala, India
[2]Academy of Scientific and Innovative Research (AcSIR), CSIR-NIIST Campus, Thiruvananthapuram, India
[3]CSIR-North East Institute of Science and Technology, Jorhat, Assam, India

Received 13 May 2015, accepted 14 August 2015, DOI: 10.1111/php.12527

ABSTRACT

Synthesis, photophysical and metal ion recognition properties of a series of amino acid-linked free-base and Zn-porphyrin derivatives (5–9) are reported. These porphyrin derivatives showed favorable photophysical properties including high molar extinction coefficients (>1 × 10^5 M^{-1} cm^{-1} for the Soret band), quantum yields of triplet excited states (63–94%) and singlet oxygen generation efficiencies (59–91%). Particularly, the Zn-porphyrin derivatives, 6 and 9 showed higher molar extinction coefficients, decreased fluorescence quantum yields, and higher triplet and singlet oxygen quantum yields compared to the corresponding free-base porphyrin derivatives. Further, the study of their interactions with various metal ions indicated that the proline-conjugated Zn-porphyrins (6 and 9) showed high selectivity toward Cu^{2+} ions and signaled the recognition through changes in fluorescence intensity. Our results provide insights on the role of nature of amino acid and metallation in the design of the porphyrin systems for application as probes and sensitizers.

INTRODUCTION

Porphyrins are macrocyclic molecular systems with a ring-shaped tetrapyrrolic core. These systems are important in various biological processes and are capable of forming complexes with a variety of metal ions (1–12). For example, heme is an iron chelate of a porphyrin, whereas chlorophyll and bacteriochlorophyll are the magnesium chelates. The porphyrin-based molecules have been extensively investigated for a variety of applications including, as sensitizers in photodynamic therapy (PDT) and solar harvesting, and as probes for metal cations and anions (9,13–18). Moreover, these systems show intense red fluorescence with good quantum yields and excellent phototoxicity thereby making them suitable candidates as photosensitizers for image-guided therapy (19–25). Photodynamic therapy, a noninvasive modality for the treatment of cancer, involves the combined interaction of oxygen, light and a photosensitizing agent, and cause local destruction of cancerous cells through the generation of reactive oxygen species (ROS) (26). Among ROS, singlet oxygen ($^1O_2$) has been postulated to be the most prevalent cytotoxic agent responsible for the photo inactivation of tumor cells by most of the sensitizers. An ideal photosensitizer should have desirable photophysical properties such as high photostability, triplet quantum yields and singlet oxygen generation efficiencies, and good absorption in the >700 nm region, where the tissues are most transparent (27,28). Porphyrins have been considered as efficient candidates for photodynamic therapeutic applications on account of their excellent photophysical properties like high triplet quantum yields and singlet oxygen generation efficiencies (28). Furthermore, the pharmacokinetic properties of sensitizers such as cellular localization and uptake are important factors which govern their efficacy in PDT applications (1,14,15,29). In this context, efforts have been made to modify the porphyrin-based sensitizers through linking with cellular recognition elements such as proteins (30–32), peptides (33–37) and sugars (38–41). Some of these porphyrin conjugates exhibited excellent photophysical as well as biological activities including DNA intercalation (42).

Another interesting aspect of the photophysics of porphyrins is their interaction with various metal ions in their free base and core metallated forms. Core metallation perturbs the photophysical properties including singlet and triplet quantum yields, and can be used as a strategy to fine-tune these properties for various applications. Similarly, the peripheral decoration of porphyrins with groups containing metal interaction motifs can be used as a strategy for sensing of biologically relevant metal ions (2,43). Herein, we have synthesized a few novel porphyrin conjugates linked with amino acids like proline and tryptophan, and evaluated their photophysical properties including absorption, fluorescence, triplet and singlet oxygen generation efficiencies. Further, the interaction of these porphyrin derivatives with biologically relevant metal ions was evaluated. Our results indicate that these porphyrin conjugates exhibit excellent quantum yields of triplet excited states and singlet oxygen generation, and show selective interactions with Cu^{2+} ions depending on the core metallation and the amino acid group present thereby demonstrating their potential as probes and sensitizers.

MATERIALS AND METHODS

Methods. All melting points are uncorrected and were determined on a Mel-Temp II melting point apparatus. ^1H and ^{13}C NMR spectra were measured on a Bruker AVANSDPX300 or Bruker AVANSII spectrometer. MALDI-TOF MS analysis was performed with a Shimadzu Biotech Axima CFR plus instrument equipped with a nitrogen laser in the linear

*Corresponding authors e-mails: joshy@niist.res.in (Joshy Joseph) and d.ramaiah@gmail.com (Danaboyina Ramaiah)

mode using 2,5-dihydroxybenzoic acid (DHB) as the matrix. The electronic absorption spectra were recorded on a Shimadzu UV-Vis-NIR spectrophotometer. Fluorescence spectra were recorded on a SPEX-Fluorolog F112X spectrofluorimeter. The transient absorption studies were carried out using a nanosecond laser flash photolysis system by employing an Applied Photophysics model LKS-20 laser kinetic spectrometer using OCR-12 Series Quanta Ray Nd:YAG laser (44,45). Quantum yields of fluorescence were measured by the relative methods using optically dilute solutions and tetraphenylporphyrin (TPP, $\Phi_F = 0.11$) was used as the standard (46). The photophysical properties of the synthesized derivatives were carried out in appropriate solvents using reported standard procedures (47,48). All experiments were carried out at room temperature (25 ± 1°C) unless otherwise mentioned.

Materials. 4-Methoxybenzaldehyde, pyrrole, trifluoroacetic acid, 2,3-dichloro-5,6-dicyano-1,4-benzoquinone (DDQ), L-proline benzyl ester, L-tryptophan methyl ester, 2-(1H-7-azabenzo-triazol-1-yl)-1,1,3,3-tetramethyluronium hexafluorophosphate (HATU), boron tribromide, *β*-carotene, hematoporphyrin, $[Ru(bpy)_3]^{2+}$ and all the metal perchlorates used for metal ion interaction were purchased from Aldrich and used as received. 1,3-Diphenylisobenzofuran (DPBF) was recrystallized from a mixture (1:3) of methanol and acetone. The standard porphyrin derivative, TPP was synthesized according to Lindsey's method (49). 4-Methoxyphenyldipyrromethane was synthesized according to the literature procedure (50). All the solvents used were purified and distilled before use.

*Synthesis of the porphyrin derivatives **1** and **2**.* 4-Methoxy-phenyldipyrromethane (3.21 mmol) and methyl 4-formylbenzoate (3.21 mmol) were dissolved in dry dichloromethane (500 mL). Trifluoroacetic acid (1.3 mmol) was added to the reaction mixture and was allowed to stir under argon atmosphere for 2 h. 2,3-Dichloro-5,6-dicyanobenzoquinone (4.8 mmol) was added, and the reaction mixture was allowed to stir further for 2 h at room temperature. The reaction mixture was filtered through an alumina column using dichloromethane. The solvent was removed under reduced pressure to give the solid residue, which was chromatographed over silica gel using chloroform as the eluent to give the systems **1** and **2** in 25% and 18%, respectively.

*5-[4-(Carboxyphenyl)phenyl]-10,15,20-tris(4-ethoxyphenyl) porphyrin (**1**, 25%).* mp > 300°C; ^{1}H NMR (300 MHz, $CDCl_3$, TMS): δ −2.76 (s, 2H), 4.09 (s, 12H), 7.28 (t, 6H, J = 8 Hz), 8.11 (m, 6H), 8.29 (d, 2H, J = 8 Hz), 8.42 (t, 2H), 8.76 (d, 8H, J = 9 Hz); ^{13}C NMR (125 MHz, $CDCl_3$): δ 52.53, 56.32, 115.26, 119.74, 127.82, 129.95, 132.54, 133.82, 134.51, 136.26, 148.73, 159.83, 165.92; FAB-MS m/z Calcd for $C_{49}H_{38}N_4O_6$: 762.42, Found: 764.28 (M + 2).

*5,15-[4-(Carboxyphenyl)phenyl]-10,20-bis(4-methoxyphenyl) porphyrin (**2**, 18%).* mp > 300°C; ^{1}H NMR (300 MHz, $CDCl_3$, TMS): δ −2.77 (s, 2H), 4.10 (s, 12H), 7.28 (q, 4H, J = 8 Hz), 8.10 (q, 4H, J = 10 Hz), 8.29 (q, 4H, J = 10 Hz), 8.43 (t, 4H, J = 10 Hz), 8.77 (dd, 8H, J = 10 Hz); ^{13}C NMR (125 MHz, $CDCl_3$): δ 51.82, 55.97, 102.95, 114.44, 121.12, 129.14, 133.28, 136.88, 142.84, 146.94, 154.73, 159.35, 164.84; FAB-MS m/z Calcd for $C_{50}H_{38}N_4O_6$: 790.14, Found: 791.94 (M + 2).

*Synthesis of monocarboxylic acid derivative of porphyrin **3**.* Boron tribromide (7.42 mmol) was added to dry dichloromethane (10 mL) and the mixture was cooled to −78°C. The porphyrin **1** (0.32 mmol) was dissolved in 10 mL of dry dichloromethane, and was slowly added to the reaction mixture over a period of 20 min. The mixture was stirred for 2 h at −78°C and then for 12 h at 25°C. After the reaction, excess of methanol was added to the reaction mixture followed by triethylamine to neutralize the reaction mixture. The solvent was removed under reduced pressure to give the purple solid, which was washed with dichloromethane, and recrystallized from a 3:1 mixture of methanol and chloroform to give 90% of the mono ester of porphyrin, which on hydrolysis with aqueous KOH (2 N) gave the porphyrin derivative **3** (85%): mp > 300°C; ^{1}H NMR (300 MHz, DMSO-d_6, TMS): δ −2.92 (s, 2H), 7.19 (d, 6H, J = 8 Hz), 7.99 (d, 6H, J = 8 Hz), 8.26 (dd, 4H, J = 7.8 Hz), 8.81 (d, 8H), 10.01 (s, 3H); ^{13}C NMR (125 MHz, CD_3OD): δ 114.81, 121.74, 126.21, 129.03-129.52, 134.07, 136.97, 137.95, 158.92, 173.11; FAB MS: m/z Calcd for $C_{45}H_{30}N_4O_5$: 706.74, Found: 708.65 (M + 2).

*Synthesis of dicarboxylic acid derivative of the porphyrin **4**.* The dicarboxylic acid porphyrin **4** was synthesized through adopting the procedure same as that of **3** (80%). mp > 300 °C; ^{1}H NMR (500 MHz, DMSO d_6, TMS): δ −3.07 (s, 2H), 7.02 (d, 4H, J = 10.5 Hz), 7.81 (d, 4H, J = 6.5 Hz), 8.01 (dd, 8H, J = 6.5 Hz), 8.65 (d, 8H), 9.97 (t_{broad}, 2H); ^{13}C NMR (125 MHz, CD_3OD): δ 114.84, 121.76, 126.21, 129.02-129.53, 134.04, 136.97, 137.92, 158.97, 173.13; FAB MS: m/z Calcd for $C_{46}H_{30}N_4O_6$: 734.01, Found: 735.23 (M + 1).

*Synthesis of the proline-linked porphyrin **5**.* The porphyrin derivative **3** (0.14 mmol) and L-proline benzyl ester (0.14 mmol) were dissolved in dry tetrahydrofuran under argon atmosphere and cooled to 0°C. 2-(1H-7-azabenzo-triazol-1-yl)-1,1,3,3-tetramethyluronium hexafluorophosphate (HATU) was added and stirred for 5 min. Then, DIPEA was added into the reaction mixture and was allowed to stir for 6 h. The reaction mixture was filtered and the solvent was removed under reduced pressure. The residue was dissolved in water and extracted with ethyl acetate. The organic layer was collected and the solvent was removed under reduced pressure. The residue obtained was chromatographed over silica gel using a methanol–chloroform mixture (1:9) as the eluent to give the porphyrin conjugate **5** (70%). mp > 300°C; ^{1}H NMR (300 MHz, DMSO-d_6, TMS): δ −2.87 (s, 2H), 2.03 (s_{broad}, 3H), 2.43 (t_{broad}, 1H), 3.90 (d_{broad}, 2H), 4.73 (t_{broad}, 1H), 5.24, (q, 2H), 7.21 (d, 6H, J = 7.5 Hz), 7.35 (m, 5H), 7.95 (d, 2H, J = 9.5 Hz), 8.00 (d, 6H, J = 7.5 Hz), 8.27 (d, 2H, J = 7.0 Hz), 8.78 (t, 8H), 9.99 (s, 3H); ^{13}C NMR (125 MHz, CD_3OD): δ 25.41, 30.19, 67.85, 71.53, 105.04, 114.82, 121.70, 126.20, 129.05-129.56, 134.06, 136.97, 137.97, 158.98, 173.17; FAB MS: m/z Calcd for $C_{57}H_{43}N_5O_6$: 893.98, Found: 895.67(M + 2).

*Synthesis of Zn complex of the proline-linked porphyrin **6**.* The porphyrin derivative **5** (0.11 mmol) was dissolved in methanol and zinc acetate (0.22 mmol) was added and stirred for 12 h. The progress of the reaction was monitored by UV spectral changes. The reaction mixture was concentrated; residue obtained was dissolved in water and extracted with ethyl acetate. The organic layer was collected, washed with several portions of water and dried over anhydrous Na_2SO_4. The solvent was removed under reduced pressure, and the residue obtained was column chromatographed over silica gel using a mixture of methanol–chloroform (3:9) as eluent to give the zinc complex **6** (65%). mp > 300°C; ^{1}H NMR (300 MHz, DMSO-d_6, TMS): δ 1.99 (m_{broad}, 3H), 2.44 (m_{broad}, 1H), 3.91 (q_{broad}, 2H), 4.73 (q_{broad}, 1H), 5.25 (q, 2H), 7.18 (d, 6H, J = 8.0 Hz), 7.36 (m, 5H), 7.94 (d, 8H, J = 8.5 Hz), 8.24 (d, 2H, J = 8.0 Hz), 8.77 (d, 8H), 9.87 (s, 3H); ^{13}C NMR (125 MHz, CD_3OD): δ 20.9, 22.45, 36.39, 47.22, 65.55, 68.39, 84.91, 99.49, 104.28, 110.99, 111.63, 113.55, 120.04, 123.38, 127.59–127.76, 128.47, 129.37, 137.87, 140.50,142.68, 145.75–145.87, 149.69, 155.07, 160.11, 165.86, 167.53, 168.27 FAB MS: m/z Calcd for $C_{57}H_{41}N_5O_6Zn$ 955.22, Found: 956.71 (M + 1).

*Synthesis of the tryptophan-linked porphyrin **7**.* The tryptophan-linked conjugate **7** was synthesized through adopting similar procedure as that of **5** and using tryptophan methyl ester (70%). mp > 300°C; ^{1}H NMR (300 MHz, DMSO-d_6, TMS): δ −2.98 (s, 2H), 1.19, (s, 2H), 3.72 (s, 3H), 4.86 (d_{broad}, 1H), 6.86 (s_{broad}, 2H), 7.01 (m, 6H), 7.33 (t, 2H), 7.63 (d, 1H), 7.96 (d, 6H, J = 8.4 Hz), 8.26 (s, 4H), 8.76, (d, 8H), 9.17 (d, 1H, J = 7.5 Hz), 9.95 (s, 3H), 10.90 (s, 1H); FAB MS: m/z Calcd for $C_{57}H_{42}N_6O_6$: 906.32, Found: 908.52 (M + 2).

*Synthesis of bis-proline-linked porphyrin **8** (60%).* mp > 300°C; ^{1}H NMR (300 MHz, DMSO-d_6, TMS): δ −2.84 (s, 2H), 2.09 (b, 6H), 2.48, (t_{broad}, 2H), 3.96 (s, 4H), 4.78 (d, 2H, J = 7.5 Hz), 5.29 (q, 4H), 7.26 (d, 4H, J = 7.5 Hz), 7.41, (m, 10H), 8.01, (dd, 8H), 8.33 (d, 4H), 8.93 (d, 8H), 10.06 (s, 2H); ^{13}C NMR (125 MHz, CD_3OD): δ 24.42, 25.29, 33.31, 59.72, 112.14, 117.72, 126.11, 128.65, 135.75, 156.61, 189.17; FAB MS: m/z Calcd for $C_{70}H_{56}N_6O_8$: 1109.23, Found: 1111.48 (M + 2).

*Synthesis of Zn complex of the bis-proline-linked porphyrin **9** (80%).* mp > 300°C; ^{1}H NMR, (300 MHz, DMSO-d_6, TMS): δ 2.01, (t_{broad}, 6H), 2.44, (t_{broad}, 2H), 3.92, (d, 4H, J = 4.5 Hz), 4.74, (t, 2H), 5.25, (q, 4H), 7.19, (d, 4H, J = 7.5 Hz), 7.38, (m, 10H), 7.95, (t, 8H), 8.25, (d, 4H, J = 7.5 Hz), 8.79, (dd, 8H), 9.87,(s, 2H); ^{13}C NMR (125 MHz, DMSO-d_6): δ 25.22, 29.00, 49.91, 59.26, 65.87, 69.62, 113.13,127.14, 128.04, 128.47, 131.87, 133.97, 135.33, 136.15, 148.82, 149.86, 156.96, 171.85; FAB-MS: m/z Calcd for $C_{70}H_{54}N_6O_8Zn$: 1172.62, Found: 1173.79 (M + 1).

Calculation of triplet excited state quantum yields. The triplet excited state yields (Φ_T) of the porphyrins were determined by an earlier reported procedure of energy transfer to *β*-carotene, using $Ru(bpy)_3^{2+}$, as the reference molecule (51). For these experiments, optically matched solutions of $Ru(bpy)_3^{2+}$ and the porphyrins at 532 nm, were mixed with a known volume of *β*-carotene solution (end concentration of *β*-carotene was fixed at *ca* 2.0×10^{-4} M). The transient absorbance of the *β* carotene triplet, generated by the energy transfer from $Ru(bpy)_3^{2+}$ or the porphyrin's triplet excited state, was monitored at 515 nm. Comparison of plateau absorbance (ΔA) following the completion of sensitized triplet formation, properly corrected for the decay of the donor triplet excited state in

competition with energy transfer to β-carotene, enabled us to estimate Φ_T of the triplet excited states based on Eq. 1.

$$\Phi_T^{por} = \Phi_T^{ref} \frac{\Delta A^{por} K_{obs}^{por} (K_{obs}^{ref} - K_0^{ref})}{\Delta A^{ref} (K_{obs}^{por} - K_0^{por}) K_{obs}^{por}} \quad (1)$$

wherein, superscripts por and ref designate various porphyrins and Ru $(bpy)_3^{2+}$, respectively, K_{obs}, is the pseudo-first-order rate constant for the growth of the β-carotene triplet and K_0 is the rate constant for the decay of the donor triplet, in the absence of β-carotene, observed in solutions containing $Ru(bpy)_3^{2+}$ or a porphyrin at the same optical density (OD = 0.1) as those used for sensitization.

Quantification of singlet oxygen generation efficiency. The quantum yields of singlet oxygen were determined by an earlier reported procedure using DPBF as the singlet oxygen scavenger (52,53). Irradiation was carried out with a light source of 200 W Hg lamp (model 3767) on an Oriel optical bench (model 11200) with a grating monochromator (model 77250). The quantum yields were measured at low dye concentrations (optical density 0.05 at the irradiation above wavelengths 495 nm) to minimize the possibility of singlet oxygen quenching by the dyes. The concentration of DPBF was $2-2.8 \times 10^{-4}$ M. Irradiations were carried out to low conversion (5–10%) of DPBF such that its concentration may be assumed to be fixed at the initial value. The photooxidation of DPBF was monitored between 0–15 s. No thermal recovery of DPBF (from a possible decomposition of endoperoxide product) was observed under the conditions of these experiments. The quantum yields of singlet oxygen generation $[\Phi(^1O_2]$ were calculated by a relative method using optically matched solutions and comparing the quantum yield of photooxidation of DPBF sensitized by the dye of interest to the quantum yield of hematoporphyrin, $[\Phi(^1O_2) = 0.74]$ sensitized DPBF photooxidation as the reference (54).

$$\phi(^1O_2)^{por} = \phi(^1O_2)^{ref} \frac{m^{por} F^{ref}}{m^{ref} F^{por}} \quad (2)$$

The quantum yields were calculated using the Eq. 2, wherein superscripts por and ref designate the porphyrin derivatives and the standard hematoporphyrin, respectively, $[\Phi(^1O_2)]$ is the quantum yield of singlet oxygen, m is the slope of a plot of change in absorbance of DPBF (at 410 nm) with the irradiation time and F is the absorption correction factor, which is given by $F = 1 - 10^{-OD}$ (OD at the irradiation wavelength).

Calculation of association constants. The association constants between the porphyrin derivatives **6** and **9** with Cu^{2+} ions were analyzed using the fluorescence data. The association constants were calculated employing Benesi–Hildebrand method, wherein Eqs. 3 and 4 were used for the porphyrin derivatives **6** and **9**, respectively (55–57).

$$\frac{1}{I - I_0} = \frac{1}{I - I_{fc}} + \frac{1}{K(I - I_{fc})[Cu^{2+}]} \quad (3)$$

$$\frac{1}{I - I_0} = \frac{1}{I - I_{fc}} + \frac{1}{K(I - I_{fc})[Cu^{2+}]^2} \quad (4)$$

where in K is the association constant, I is the fluorescence intensity of the free porphyrin, I_0 is the observed fluorescence intensity of the [**6**/**9**-Cu^{2+}] complex and I_{fc} is the fluorescence intensity at the saturation point.

RESULTS AND DISCUSSION

Synthesis and photophysical properties

The synthesis of the amino acid-conjugated porphyrin derivatives and their metal complexes has been achieved as shown in Scheme 1. The condensation reaction of 4-formyl-methylbenzoate with 4-methoxyphenyldipyrromethane using trifluoroacetic acid in dry methylene chloride followed by oxidation with DDQ gave the porphyrin derivatives **1** and **2** in 25% and 18% yields. The hydrolysis of these derivatives with boron tribromide in dry methylene chloride followed by base hydrolysis gave the porphyrin derivatives **3** and **4** in 85% and 80%, respectively. On the other hand, the synthesis of amino acid-linked porphyrin derivatives **5**, **7** and **8** was achieved by the reaction of the acid-substituted porphyrin derivatives with proline benzyl ester and tryptophan methyl ester, respectively, in the presence of 2-(1H-7-azabenzotriazol-1-yl)-1,1,3,3-tetramethyl uronium hexafluorophosphate (HATU) and diisopropylethylamine (DIPEA) in dry tetrahydrofuran. The zinc complexes of these amino acid-conjugated porphyrin derivatives **6** and **9** were synthesized by the reaction of these free-base porphyrins with zinc acetate in methanol. All the starting materials and porphyrin derivatives were characterized by various spectroscopic techniques and analytical evidence (Figures S1–S9, Supporting Information).

Figure 1 shows the absorption spectra of the proline-conjugated free-base porphyrin **5** and its Zn complex **6**. The porphyrin **5** showed characteristic Soret band at 417 nm, while four Q-bands were observed in the region 500–700 nm. The Zn complex **6**, on the other hand exhibited a bathochromically shifted (*ca* 7 nm) Soret absorption at 424 nm and two Q-bands at 555 and 595 nm. In the fluorescence spectrum of the porphyrin **5**, we observed two characteristic emission peaks at 656 and 723 nm while its Zn complex **6** showed emission peaks, which were centered at 611 and 663 nm (Fig. 2). Similar observations were made with the tryptophan and bis-proline-linked conjugates **7–9**. The fluorescence quantum yields (Φ_F) of these porphyrin conjugates were calculated using TPP as the reference compound. The free-base amino acid-linked porphyrins showed Φ_F values in the order 0.12–0.15 $\pm$ 0.01, while quenched values of 0.04 and 0.05 $\pm$ 0.01 were observed for the Zn complexes **6** and **9**, respectively, and the photophysical characteristics of all conjugates are summarized in Table 1.

To understand the transient intermediates involved in these systems, we have carried out nanosecond laser flash photolysis studies employing a 532 nm laser pulse excitation. Figure 3 shows the transient absorption spectrum of the proline-linked porphyrin **5** obtained after the laser excitation in methanol. The transient absorption spectrum showed maximum at 450 nm with bleach at 420 nm, where the compound has significant ground state absorption. The lifetime of the transient was determined from the decay profile (Inset of Fig. 3) and it was found to be 6.8 μs. The transient observed in the case of the conjugate **5** was attributed to the formation of the triplet excited state due its quenching by the dissolved oxygen and on the basis of literature reports (24,25). Similar observations were made with other porphyrin conjugates and which too showed triplet excited state absorption maximum in the region 450–460 nm with lifetime values in the range 5–28 μs (Figure S10, Supporting Information). The quantum yields of triplet excited states (Φ_T) of these porphyrin derivatives were estimated using triplet–triplet energy transfer method to β-carotene and $[Ru(bpy)_3]^{2+}$ as the standard. These values in methanol are 0.82, 0.73, 0.91, 0.77, 0.74, 0.63 and 0.94, for the porphyrin conjugates **3–9**, respectively.

To estimate the efficacy of these conjugates as sensitizers in generating the highly reactive singlet oxygen, which has a vital role in PDT and photooxygenation reactions, we have determined quantum yields $[\Phi(^1O_2)]$ of singlet oxygen by using DPBF as the singlet oxygen scavenger. To calculate the singlet oxygen generation yields, the porphyrin conjugates along with DPBF was irradiated using a mercury lamp with a 495 nm long

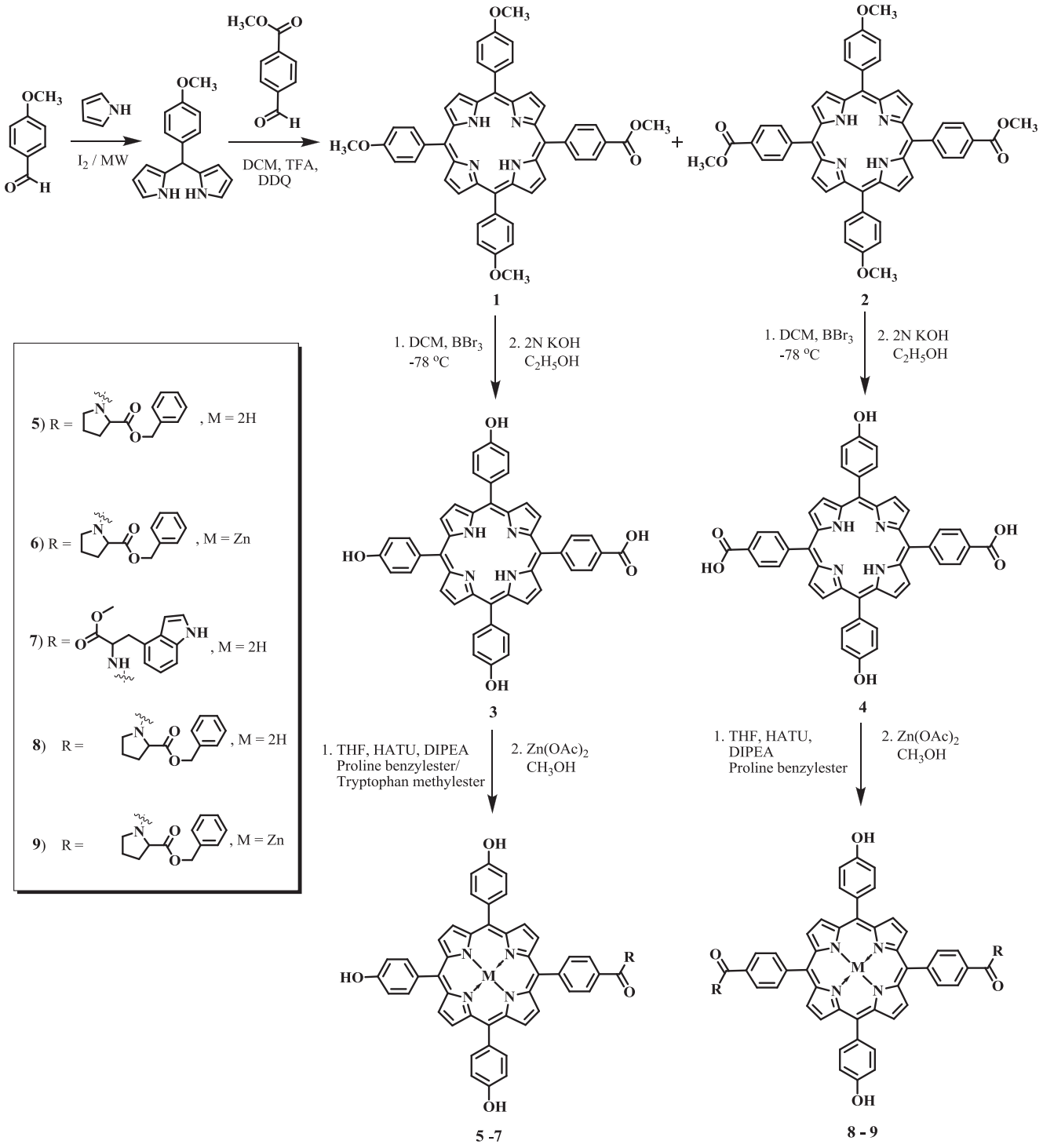

Scheme 1. Synthesis of the amino acid-conjugated porphyrin derivatives and their zinc complexes **3**–**9.**

pass filter at different time intervals from 0–15 s (Fig. 4). The decrease in the absorbance of DPBF was monitored at 410 nm and was compared with those observed with the standard, hematoporphyrin (Hp) under identical conditions. From the slope of the graph obtained by plotting the change in absorbance of DPBF against the time of irradiation (Inset of Fig. 4 and Figure S11, Supporting Information), we have calculated the singlet oxygen generation yields and the obtained values are 0.77, 0.65, 0.87, 0.72, 0.70, 0.59 and 0.91, respectively, for the porphyrin conjugates 3–9.

Investigation of interactions with metal ions

To evaluate the potential of these conjugates as metal ion probes, we have investigated their interactions with various mono- and divalent metal ions such as Na^+, K^+, Ba^{2+}, Ca^{2+}, Mn^{2+}, Mg^{2+},

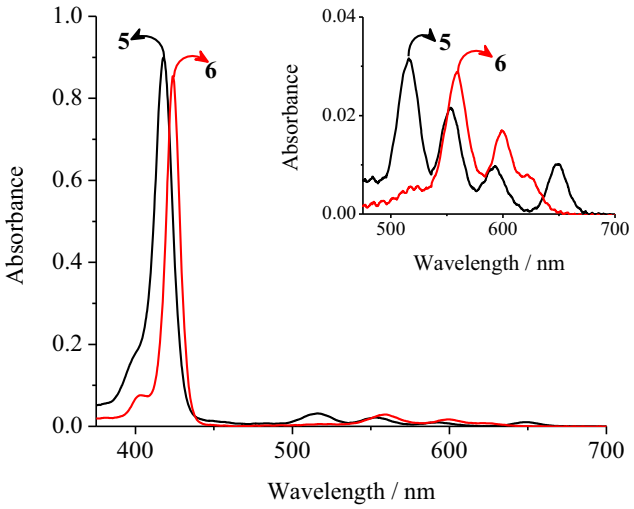

Figure 1. UV-Vis absorption spectra of the amino acid-linked free-base porphyrin derivative **5** (2.66 μM) and its zinc complex **6** (1.7 μM) in methanol. Inset shows the expanded region of Q–bands.

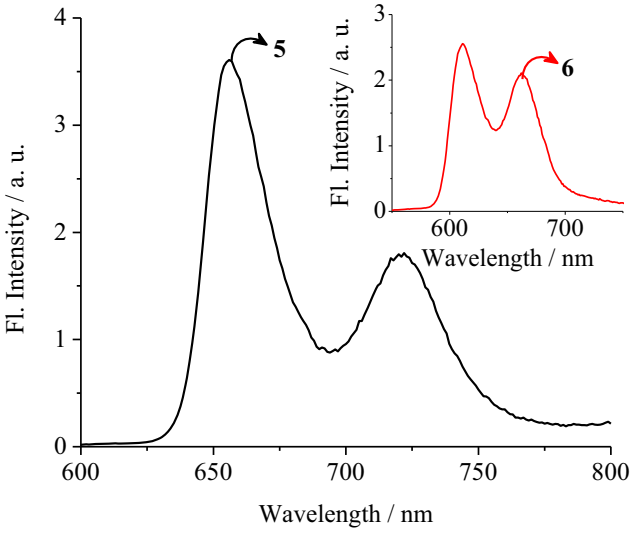

Figure 2. Fluorescence spectra of the proline-conjugated free-base porphyrin derivative **5** (2.66 μM) and its zinc complex **6** (inset) (1.7 μM) in methanol. λ_{ex}, 435 nm.

Zn^{2+}, Cd^{2+}, Co^{2+}, Hg^{2+}, Ni^{2+}, Pb^{2+} and Cu^{2+} through the absorption and fluorescence spectroscopy. Figure 5 shows the changes in the absorption spectra of the proline-linked zinc porphyrin conjugate **6** with the increase in addition of Cu^{2+} ions. As the concentration of Cu^{2+} ions increased from 0 to 18 μM, we observed a regular decrease in Soret band (*ca* 87% hypochromicity) at 424 nm with a concomitant increase in absorbance at 465 nm having an isosbestic point at 435 nm. In the emission spectrum, we observed almost complete quenching in fluorescence intensity of the conjugate **6,** with the addition of 18 μM of Cu^{2+} ions (Inset of Fig. 5). Similar observations were also made with the bis-proline-linked porphyrin conjugate **9**, where we observed *ca* 93% hypochromicity at Soret band and *ca* 100% quenching in fluorescence intensity (Figure S12, Supporting Information). These observations lead to the visual fluorescence change from intense red emission to negligible emission of the conjugates **6** and **9** in the presence of Cu^{2+} ions. Similar quenching effect was observed in the phosphorescence emission spectra of **6** in presence of Cu(II) ions ((Figure S17, Supporting Information).

The absorption and fluorescence changes of the Zn complexes of proline-linked porphyrin conjugates **6** and **9** in the presence of Cu^{2+} ions were analyzed through Job's and Benesi–Hildebrand plots (Figures S15–S16 Supporting information). These analyses gave 1:1 and 1:2 stoichiometry, respectively, for the complexes between Cu^{2+} ions and the conjugates **6** and **9** with association constant (K_{ass}) values of $4.2 \pm 0.1 \times 10^5$ M^{-1} and $2.2 \pm 0.1 \times 10^{11}$ M^{-2}, respectively. We carried similar titration experiments with the tryptophan-linked porphyrin conjugate **7** and it showed negligible interactions with Cu^{2+} ions, even at higher concentrations (50 μM) (Figure S13, Supporting Information).

On the other hand, the mono and bis-proline-linked free-base porphyrins **5** and **8** showed a gradual decrease in Soret band at 424 nm (*ca* 95%) with a concomitant increase in absorbance at 462 nm.

However, we observed only marginal changes in fluorescence intensity with the increase in addition of Cu^{2+} ions from 0 to 18 μM (Figures S14 Supporting Information).

To determine the selectivity of recognition, we have investigated the interactions of the proline-linked conjugates **6** and **9** with other environmentally important metal ions such as K^+, Ba^{2+}, Ca^{2+}, Mn^{2+}, Mg^{2+}, Zn^{2+}, Cd^{2+}, Co^{2+}, Hg^{2+}, Ni^{2+} and Pb^{2+}. Figure 6 shows the relative changes in the fluorescence intensity of these conjugates with the gradual addition of similar

Table 1. Photophysical properties of the free-base and Zn-porphyrin derivatives, **3 9**.*,†

Porphyrin Conjugate	λ_{ab} (nm)	ε (M^{-1} cm^{-1})	λ_{em} (nm)	Φ_F	Φ_T	τ_T (μs)	$\Phi(^1O_2)$
3	417	1.03×10^5	653	0.12 ± 0.02	0.82 ± 0.02	10.82	0.77 ± 0.02
	645	1.81×10^3	724				
4	417	1.45×10^5	656	0.12 ± 0.02	0.74 ± 0.02	9.14	0.70 ± 0.02
	649	1.47×10^3	723				
5	417	3.35×10^5	656	0.13 ± 0.02	0.73 ± 0.02	6.84	0.65 ± 0.02
	649	4.73×10^3	723				
6	424	5.24×10^5	611	0.06 ± 0.01	0.91 ± 0.02	26.7	0.87 ± 0.02
	596	3.84×10^3	663				
7	417	2.93×10^5	655	0.14 ± 0.02	0.77 ± 0.02	8.86	0.72 ± 0.02
	647	1.83×10^3	724				
8	417	1.87×10^5	755	0.15 ± 0.02	0.63 ± 0.02	13.68	0.59 ± 0.02
	649	1.23×10^3	724				
9	424	5.43×10^5	610	0.04 ± 0.01	0.94 ± 0.01	27.09	0.91 ± 0.02
	598	8.41×10^3	662				

*Average of more than three independent experiments. †Error involved in lifetime measurements is <5%.

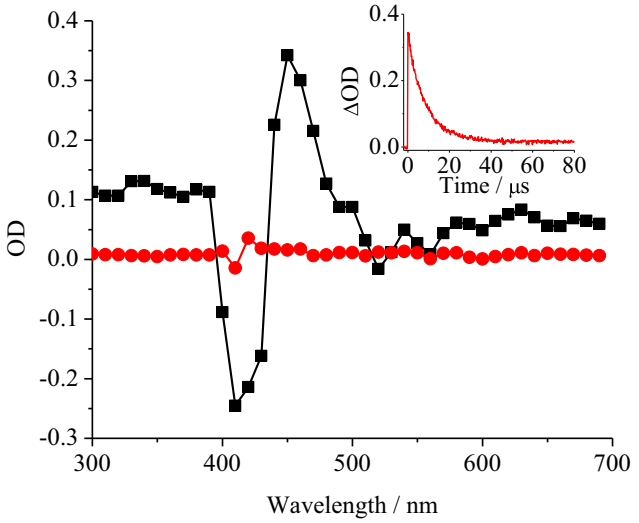

Figure 3. Transient absorption spectra of the proline-conjugated free-base porphyrin **5** (OD = 0.1 at 532 nm) following the laser pulse (532 nm) excitation in methanol at (■) 0.6 and (●) 80 μs. Inset shows the decay of the transient at 450 nm in methanol.

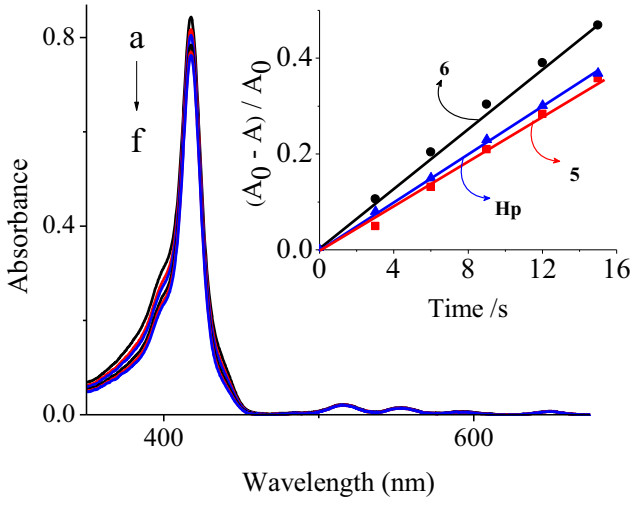

Figure 4. Changes in absorbance of 1,3-diphenylisobenzofuran (DPBF, 0.2 mM) upon irradiation (515 nm LP) in presence of the porphyrin conjugate **5** (2.1 μM) in methanol. a = 0 s and f = 15 s. Inset shows the plot of change in absorption of DPBF *vs* irradiation time in presence of the conjugates **5, 6** and the standard, hematoporphyrin (Hp) using similar and optically matched solutions.

concentrations of different metal ions. As can be seen from Fig. 6, the addition of these metal ions showed negligible changes in the fluorescence intensity of the porphyrin conjugates **6** and **9**. This unusual selectivity of the conjugates toward Cu^{2+} ions can be observed visually through the quenching of the intense red fluorescence, whereas no such change was observed with the addition of other metal ions.

As evidenced by fluorescence (Fig. 7) and UV-Vis spectral changes, the selective detection of Cu^{2+} was possible only through the proline-Zn-porphyrin conjugates **6** and **9**, which clearly indicate the importance of the two keto groups of the proline conjugates and the central Zn^{2+} ion for the complexation with Cu^{2+} ions.

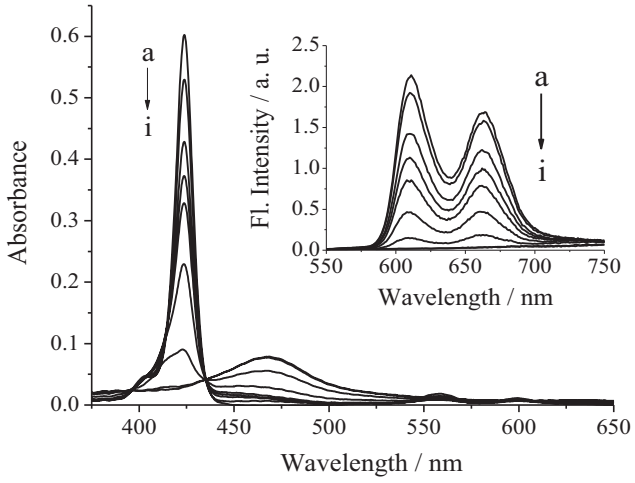

Figure 5. Changes in the absorption and fluorescence (inset) spectra of the porphyrin derivative **6** (1.2 μM) in the presence of various concentrations of Cu^{2+} ions in acetonitrile. a = 0 μM of Cu^{2+} ions and I = 18 μM of Cu^{2+} ions. λ_{ex}, 435 nm.

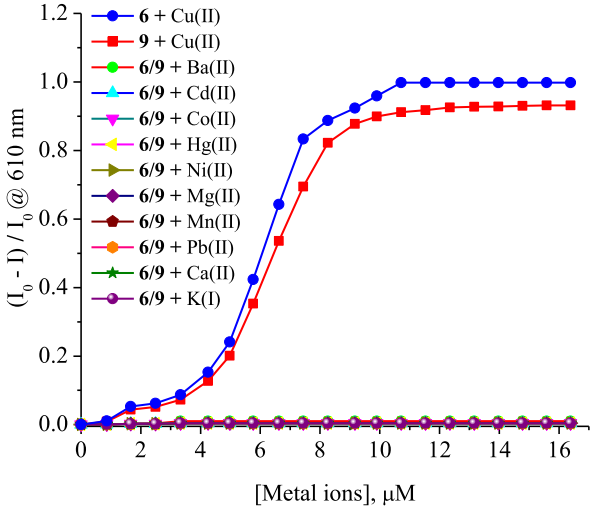

Figure 6. Relative fluorescence changes of the Zn complexes of the proline-linked porphyrin derivatives **6** (1.7 μM) and **9** (1.7 μM) with the addition of various concentrations of metal ions in acetonitrile under identical conditions. λ_{ex}, 435 nm.

CONCLUSIONS

In conclusion, we synthesized a few amino acid-conjugated porphyrin derivatives and their zinc complexes, and have investigated their photophysical and metal ion recognition properties. These systems exhibited absorption and fluorescence spectra characteristic of the porphyrin chromophore. The nanosecond laser studies revealed that these systems show triplet excited states as the major transient intermediates which sensitize the generation of singlet oxygen in excellent yields. Further, the study of interactions of these porphyrin derivatives with various metal ions showed that, among the various systems, the zinc complexes of the proline-linked porphyrin derivatives exhibit selectivity toward Cu^{2+} ions resulting in visual fluorescence changes. The results reveal that the nature of amino acid and metallation play major roles in the interactions of these systems

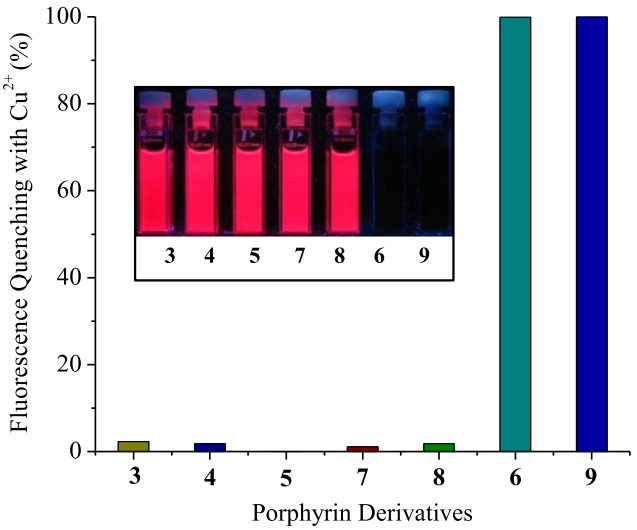

Figure 7. Selectivity plot of Cu^{2+} ions recognition. The Zn complexes of the porphyrin conjugates **6** and **9** showed selectivity towards Cu^{2+} ions when compared to the conjugates **3–5** and **7–8**. Inset shows the visual fluorescence changes of all the derivatives **3–9** in the presence of Cu^{2+} ions (18 μM). λ_{ex}, 435 nm.

with metal ions, and also in generating singlet oxygen thereby their potential use as sensitizers in PDT and photooxygenation reactions.

Acknowledgements—We acknowledge the financial support from CSIR-M2D Program and DST, Government of India. A. K. P. thank CSIR for Research Fellowship and J.J. thank DST for Ramanujan Fellowship. This is contribution no. PPG–347 from CSIR-NIIST, Thiruvananthapuram.

SUPPORTING INFORMATION

Additional Supporting Information may be found in the online version of this article:

Figures S1-S9. The ^{1}H NMR spectra of **1** to **9.**

Figure S10. Triplet absorption spectra of the porphyrin **3**.

Figure S11. Plot of change in absorption of DPBF vs irradiation time in presence of porphyrins **3, 4** and **7 9** and the standard, hematoporphyrin (Hp).

Figure S12. Changes in absorption and fluorescence spectra of the zinc complex of bis-proline-conjugated porphyrin 7.

Figure S13. Changes in absorption and fluorescence spectra of the tryptophan-linked porphyrin 6 with Cu^{2+} ions.

Figure S14. Changes in absorption and fluorescence spectra of the mono-proline-conjugated porphyrin 5 with Cu^{2+} ions.

Figure S15. Job's plot and Benesi–Hildebrand fit for the binding of Cu(ClO4)2 with the porphyrin derivative 6.

Figure S16. Job's plot and the Benesi–Hildebrand fit for the binding of Cu(ClO4)2 with the porphyrin derivative 9.

Figure S17. Phosphorescence spectra of the porphyrin derivative 6 alone (1.5 μM) and in presence of Cu (II) ions (18 μM).

REFERENCES

1. Bonnett, R. (1995) Photosensitizers of the porphyrin and phthalocyanine series for photodynamic therapy. *Chem. Soc. Rev.* **24**, 19–33.
2. Weng, Y. Q., F. Yue, Y. R. Zhong and B. H. Ye (2007) A Copper (II) ion-selective on-off-type fluoroionophore based on zinc porphyrin-dipyridylamino. *Inorg. Chem.* **46**, 7749–7755.
3. Boitrel, B. (2010) Bismuth complexes of porphyrins and their potential in medical applications. *In Biological Chemistry of Arsenic, Antimony and Bismuth*. (Edited by. H. Sun), pp. 209–240. John Wiley & Sons, Ltd., Chichester, UK.
4. Nowostawska, M., S. Corr, S. Byrne, J. Conroy, Y. Volkov and Y. Gun'ko (2011) Porphyrin-magnetite nanoconjugates for biological imaging. *J. Nanobiotechnol.* **9**, 13.
5. Brothers, P. J. and J. P. Collman (1986) The organometallic chemistry of transition-metal porphyrin complexes. *Acc. Chem. Res.* **19**, 209–215.
6. Lemon, C. M., P. J. Brothers and B. Boitrel (2011) Porphyrin complexes of the period 6 main group and late transition metals. *Dalton Trans.* **40**, 6591–6609.
7. Huang, X. F., K. Nakanishi and N. Berova (2000) Porphyrins and metalloporphyrins: Versatile circular dichroic reporter groups for structural studies. *Chirality* **12**, 237–255.
8. Sternberg, E. D., D. Dolphin and C. Brückner (1998) Porphyrin-based photosensitizers for use in photodynamic therapy. *Tetrahedron* **54**, 4151–4202.
9. Ding, Y. B., Y. Y. Tang, W. H. Zhu and Y. S. Xie (2015) Fluorescent and colorimetric ion probes based on conjugated oligopyrroles. *Chem. Soc. Rev.* **44**, 1101–1112.
10. Tanaka, T. and A. Osuka (2015) Conjugated porphyrin arrays: Synthesis, properties and applications for functional materials. *Chem. Soc. Rev.* **44**, 943–969.
11. Labuta, J., J. P. Hill, S. Ishihara, L. Hanykova and K. Ariga (2015) Chiral sensing by nonchiral tetrapyrroles. *Acc. Chem. Res.* **48**, 521–529.
12. Alves, E., M. A. F. Faustino, M. G. P. M. S. Neves, A. Cunha, H. Nadais and A. Almeida (2015) Potential applications of porphyrins in photodynamic inactivation beyond the medical scope. *J. Photochem. Photobiol., C* **22**, 34–57.
13. Nitzan, Y., M. Gutterman, Z. Malik and B. Ehrenberg (1992) Inactivation of gram-negative bacteria by photosensitized porphyrins. *Photochem. Photobiol.* **55**, 89–96.
14. Ethirajan, M., Y. Chen, P. Joshi and R. K. Pandey (2011) The role of porphyrin chemistry in tumor imaging and photodynamic therapy. *Chem. Soc. Rev.* **40**, 340–362.
15. O'Connor, A. E., W. M. Gallagher and A. T. Byrne (2009) Porphyrin and nonporphyrin photosensitizers in oncology: Preclinical and clinical advances in photodynamic therapy. *Photochem. Photobiol.* **85**, 1053–1074.
16. Urbani, M., M. Grätzel, M. K. Nazeeruddin and T. Torres (2014) Meso-substituted porphyrins for dye-sensitized solar cells. *Chem. Rev.* **114**, 12330–12396.
17. Walter, M. G., A. B. Rudine and C. C. Wamser (2010) Porphyrins and phthalocyanines in solar photovoltaic cells. *J. Porphyrins Phthalocyanines* **14**, 759–792.
18. Moura, N. M. M., C. Núñez, S. M. Santos, M. A. F. Faustino, J. A. S. Cavaleiro, M. G. P. M. S. Neves, J. L. Capelo and C. Lodeiro (2013) Functionalized porphyrins as red fluorescent probes for metal cations: Spectroscopic, MALDI-TOF spectrometry, and doped-polymer studies. *ChemPlusChem* **78**, 1230–1243.
19. Liang, X. L., X. D. Li, L. J. Jing, X. L. Yue and Z. F. Dai (2014) Theranostic porphyrin dyad nanoparticles for magnetic resonance imaging guided photodynamic therapy. *Biomaterials* **35**, 6379–6388.
20. Luo, J., L. F. Chen, P. Hu and Z. N. Chen (2014) Tetranuclear gadolinium(III) porphyrin complex as a theranostic agent for multimodal imaging and photodynamic therapy. *Inorg. Chem.* **53**, 4184–4191.
21. Lin, J., S. J. Wang, P. Huang, Z. Wang, S. H. Chen, G. Niu, W. W. Li, J. He, D. X. Cui, G. M. Lu, X. Y. Chen and Z. H. Nie (2013) Photosensitizer-loaded gold vesicles with strong plasmonic coupling effect for imaging-guided photothermal/photodynamic therapy. *ACS Nano* **7**, 5320–5329.
22. Hsu, C. Y., M. P. Nieh and P. S. Lai (2012) Facile self-assembly of porphyrin-embedded polymeric vesicles for theranostic applications. *Chem. Commun.* **48**, 9343–9345.
23. Zhang, Y. and J. F. Lovell (2012) Porphyrins as theranostic agents from prehistoric to modern times. *Theranostics* **2**, 905–915.

24. Avirah, R. R., D. T. Jayaram, N. Adarsh and D. Ramaiah (2012) Squaraine dyes in PDT: From basic design to in vivo demonstration. *Org. Biomol. Chem.* **10**, 911–920.
25. Karunakaran, S. C., P. S. S. Babu, B. Madhuri, B. Marydasan, A. K. Paul, A. S. Nair, K. S. Rao, A. Srinivasan, T. K. Chandrashekar, C. M. Rao, R. Pilai and D. Ramaiah (2013) In vitro demonstration of apoptosis mediated photodynamic activity and nir nucleus imaging through a novel porphyrin. *ACS Chem. Biol.* **8**, 127–132.
26. Dolmans, D. E. J. G. J., D. Fukumura and R. K. Jain (2003) Photodynamic therapy for cancer. *Nat. Rev. Cancer* **3**, 380–387.
27. Detty, M. R., S. L. Gibson and S. J. Wagner (2004) Current clinical and preclinical photosensitizers for use in photodynamic therapy. *J. Med. Chem.* **47**, 3897–3915.
28. Huang, Z. (2005) A review of progress in clinical photodynamic therapy. *Technol. Cancer Res. Treat.* **4**, 283–293.
29. Thomas, A. P., P. S. S. Babu, S. A. Nair, S. Ramakrishnan, D. Ramaiah, T. K. Chandrashekar, A. Srinivasan and M. R. Pillai (2012) Meso-Tetrakis(p-sulfonatophenyl)N-confused porphyrin tetrasodium salt: A potential sensitizer for photodynamic therapy. *J. Med. Chem.* **55**, 5110–5120.
30. Sutton, J. M., O. J. Clarke, N. Fernandez and R. W. Boyle (2002) Porphyrin, chlorin, and bacteriochlorin isothiocyanates: Useful reagents for the synthesis of photoactive bioconjugatest. *Bioconjug. Chem.* **13**, 249–263.
31. Giuntini, F., C. M. A. Alonso and R. W. Boyle (2011) Synthetic approaches for the conjugation of porphyrins and related macrocycles to peptides and proteins. *Photochem. Photobiol. Sci.* **10**, 759–791.
32. Conlon, K. A. and M. Berrios (2007) Site-directed photoproteolysis of 8-oxoguanine DNA glycosylase 1 (OGG1) by specific porphyrin-protein probe conjugates: A strategy to improve the effectiveness of photodynamic therapy for cancer. *J. Photochem. Photobiol., B* **87**, 9–17.
33. Geier Iii, G. R. and T. Sasaki (1997) The design, synthesis and characterization of a porphyrin-peptide conjugate. *Tetrahedron Lett.* **38**, 3821–3824.
34. Bhupathiraju, N. V. S. D. K., X. K. Hu, Z. H. Zhou, F. R. Fronczek, P. O. Couraud, I. A. Romero, B. Weksler and M. G. H. Vicente (2014) Synthesis and in vitro evaluation of BBB permeability, tumor cell uptake, and cytotoxicity of a series of carboranylporphyrin conjugates. *J. Med. Chem.* **57**, 6718–6728.
35. Mukai, H., Y. Wada and Y. Watanabe (2013) The synthesis of Cu-64-chelated porphyrin photosensitizers and their tumor-targeting peptide conjugates for the evaluation of target cell uptake and PET image-based pharmacokinetics of targeted photodynamic therapy agents. *Ann. Nucl. Med.* **27**, 625–639.
36. Sehgal, I., M. Sibrian-Vazquez and M. G. H. Vicente (2008) Photoinduced cytotoxicity and biodistribution of prostate cancer cell-targeted porphyrins. *J. Med. Chem.* **51**, 6014–6020.
37. Sibrian-Vazquez, M., T. J. Jensen, R. P. Hammer and M. G. H. Vicente (2006) Peptide-mediated cell transport of water soluble porphyrin conjugates. *J. Med. Chem.* **49**, 1364–1372.
38. Cavaleiro, J. A. S., M. A. F. Faustino and J. P. C. Tome (2009) Porphyrinyl-type sugar derivatives: Synthesis and biological applications. *In Carbohydrate Chemistry: Volume 35*, Vol. 35. (Edited by. A. P. Rauter and T. Lindhorst). pp. 199–231. The Royal Society of Chemistry, Cambridge, UK.
39. Giuntini, F., F. Bryden, R. Daly, E. M. Scanlan and R. W. Boyle (2014) Huisgen-based conjugation of water-soluble porphyrins to deprotected sugars: Towards mild strategies for the labelling of glycans. *Org. Biomol. Chem.* **12**, 1203–1206.
40. Casiraghi, G., M. Cornia, F. Zanardi, G. Rassu, E. Ragg and R. Bortolini (1994) Synthesis and characterization of porphyrin-sugar carbon conjugates. *J. Org. Chem.* **59**, 1801–1808.
41. Hao, E., T. J. Jensen and M. G. H. Vicente (2009) Synthesis of porphyrin-carbohydrate conjugates using "click" chemistry and their preliminary evaluation in human HEp2 cells. *J. Porphyrins Phthalocyanines* **13**, 51–59.
42. Biron, E. and N. Voyer (2005) Synthesis of cationic porphyrin modified amino acids. *Chem. Commun.*, 4652–4654.
43. Moura, N. M. M., C. Núñez, S. M. Santos, M. A. F. Faustino, J. A. S. Cavaleiro, M. G. P. M. S. Neves, J. L. Capelo and C. Lodeiro (2014) Synthesis, spectroscopy studies, and theoretical calculations of new fluorescent probes based on pyrazole containing porphyrins for Zn(II), Cd(II), and Hg(II) optical detection. *Inorg. Chem.* **53**, 6149–6158.
44. Jisha, V. S., K. T. Arun, M. Hariharan and D. Ramaiah (2006) Site-selective binding and dual mode recognition of serum albumin by a squaraine dye. *J. Am. Chem. Soc.* **128**, 6024–6025.
45. Sajimon, M. C., D. Ramaiah, K. G. Thomas and M. V. George (2001) Biradical intermediates in the photoisomerization of dibenzodihydropentalenofurans to dibenzosemibullvalenes. *J. Org. Chem.* **66**, 3182–3187.
46. Quimby, D. J. and F. R. Longo (1975) Luminescence studies on several tetraarylporphins and their zinc derivatives. *J. Am. Chem. Soc.* **97**, 5111–5117.
47. Adarsh, N., M. Shanmugasundaram, R. R. Avirah and D. Ramaiah (2012) Aza-BODIPY derivatives: Enhanced quantum yields of triplet excited states and the generation of singlet oxygen and their role as facile sustainable photooxygenation catalysts. *Chem. Eur. J.* **18**, 12655–12662.
48. Marydasan, B., A. K. Nair and D. Ramaiah (2013) Dye encapsulation and release by a zinc-porphyrin pincer system through morphological transformations. *RSC Adv.* **3**, 3815–3818.
49. Lindsey, J. S., I. C. Schreiman, H. C. Hsu, P. C. Kearney and A. M. Marguerettaz (1987) Rothemund and Adler-Longo reactions revisited - synthesis of tetraphenylporphyrins under equilibrium conditions. *J. Org. Chem.* **52**, 827–836.
50. Faugeras, P. A., B. Boens, P. H. Elchinger, J. Vergnaud, K. Teste and R. Zerrouki (2010) Synthesis of meso-substituted dipyrromethanes using iodine-catalysis. *Tetrahedron Lett.* **51**, 4630–4632.
51. Kumar, C. V., L. Qin and P. K. Das (1984) Aromatic thioketone triplets and their quenching behaviour towards oxygen and di-t-butylnitroxy radical. A laser-flash-photolysis study. *J. Chem. Soc., Faraday Trans.* **2**(80), 783–793.
52. Ahmad, M., M. D. Rahn and T. A. King (1999) Singlet oxygen and dye-triplet-state quenching in solid-state dye lasers consisting of Pyrromethene 567-doped poly(methyl methacrylate). *Appl. Opt.* **38**, 6337–6342.
53. Lindig, B. A., M. A. J. Rodgers and A. P. Schaap (1980) Determination of the lifetime of singlet oxygen in water-d2 using 9,10-anthracenedipropionic acid, a water-soluble probe. *J. Am. Chem. Soc.* **102**, 5590–5593.
54. Redmond, R. W. and J. N. Gamlin (1999) A compilation of singlet oxygen yields from biologically relevant molecules. *Photochem. Photobiol.* **70**, 391–475.
55. Avirah, R. R., K. Jyothish and D. Ramaiah (2007) Dual-mode semi-squaraine-based sensor for selective detection of Hg2 + in a micellar medium. *Org. Lett.* **9**, 121–124.
56. Karunakaran, S. C., A. K. Paul and D. Ramaiah (2014) Effective discrimination of GTP from ATP by a cationic tentacle porphyrin through "turn-on" fluorescence intensity. *RSC Adv.* **4**, 30644–30647.
57. Benesi, H. A. and J. H. Hildebrand (1949) A spectrophotometric investigation of the interaction of iodine with aromatic hydrocarbons. *J. Am. Chem. Soc.* **71**, 2703–2707.